

#### Available online at www.sciencedirect.com

## **ScienceDirect**

Transportation Research Procedia 38 (2019) 709-729



23rd International Symposium on Transportation and Traffic Theory, ISTTT 23, 24-26 July 2019, Lausanne, Switzerland

# Traffic dynamics under speed disturbance in mixed traffic with automated and non-automated vehicles

Danjue Chena, Anupam Srivastavab, Soyoung Ahnb\*, Tienan Lia

<sup>a</sup>Department of Civil and Environmental Engineering, University of Massachusetts, Lowell, United States <sup>b</sup>Department of Civil and Environmental Engineering, University of Wisconsin, Madison, United States

#### Abstract

This paper elucidates the impacts of vehicle heterogeneity on traffic dynamics and throughput of mixed traffic consisting of connected automated vehicles (CAVs) and regular vehicles (RVs). The main premise is that the heterogeneity in preferred acceleration rate, desired speed, and car-following (CF) behavior (e.g., reaction pattern and sensitivity to a traffic disturbance) will change traffic properties in ways that can undermine traffic flow throughput. This paper first decomposes the mechanism into two elements — one driven by acceleration and one by time-varying CF response to disturbances — and then investigates their compounded effect. This paper also provides unifying frameworks to analyze the behavior of RVs and CAVs to facilitate analytical investigations. The results reveal how heterogeneous acceleration and CF behavior may create persistent voids and diminish traffic throughput. Integrating all the elements, throughput reduction is quantified via numerical simulations.

© 2019 The Authors. Published by Elsevier B.V.

Peer-review under responsibility of the scientific committee of the 23rd International Symposium on Transportation and Traffic Theory.

Keywords: Transition dynamics; traffic throughput, mixed traffic; heterogeneity; connected and autonomous vehicles; chained asymmetric behavior

#### 1 Introduction

A firm understanding of driving behavior and the resulting traffic dynamics under various disturbances (temporary drops in vehicle speed) has been a cornerstone for traffic flow theory for decades. While there is a long history of modeling frameworks that describe traffic dynamics, we have only a limited understanding of transition dynamics in heterogenous freeway traffic under systematic disturbances (e.g., arising from merging/diverging flow). A disturbance may undermine the traffic throughput and alter traffic properties, which in turn, affect traffic performance under subsequent disturbances.

Interest in Connected and Autonomous Vehicles (CAVs) has been growing exponentially in recent years, with increasing levels of automation being introduced to newer vehicles on the road. Due to the wide range of potential

<sup>\*</sup> Corresponding author. Tel.: +1-608-265-9067; fax: +1-608-262-5199. E-mail address: ahn37@wisc.edu

applications, control objectives and control logic, the behavior of CAVs can vary significantly from one another and from non-automated vehicles (referred to as 'regular' vehicles (RVs), hereafter). Mixed traffic streams composed of a variety of CAVs and RVs thus lead to a highly heterogeneous environment, that can have a major impact on roadway throughput and traffic dynamics, particularly when the mixed traffic is perturbed by disturbances. The involved traffic dynamics in this heterogeneous environment can have profound implications for the benefits that can be derived from CAV technologies and for control and management strategies to improve traffic performance (e.g., ramp metering, variable speed limits, signal control, etc.). Yet, the impacts of heterogeneity in mixed vehicular traffic, particularly the technology-induced heterogeneity, on key dynamic traffic features remain elusive.

Traffic disturbances are ubiquitous on roadway networks, triggered either by (forced or cooperative) lane changes, or by instability in car-following (such as stop-and-go triggered by rubbernecking). Recurring disturbances are often responsible for instigating persistent congestion and significantly undermining throughput (Chen et al. 2014; Knoop et al., 2008; Knoop et al., 2009). Periodic disturbances like stop-and-go oscillations often grow as they propagate upstream: subtle speed variations evolve to complete stoppage of traffic as they propagate through vehicles. The mechanisms of such traffic phenomena, capacity drop and stop-and-go waves, have been well researched. For capacity drop, the seminal work by Laval and Daganzo (2006) postulated that a lane change near a merge bottleneck creates an irreversible 'void' (extra time or space gap) ahead due to finite acceleration. In contrast, (Chen et al., 2012) conjectured that a void can emerge by time-dependent response time while experiencing a disturbance. Both studies reproduced capacity drop values consistent with field observations, suggesting that both premises are plausible. Furthermore, disturbance amplification has been linked to lane changes (Mauch and Cassidy, 2002; Ahn and Cassidy, 2007; Zheng et al., 2013) and time-dependent response time (Chen et al., 2014), which is well captured by the asymmetric behavioral (AB) model (Chen et al. 2012a).

There exist three major approaches for CAV longitudinal control: linear controller (e.g., Naus et al., 2010; Öncü et al., 2014; Swaroop et al., 1994; Swaroop and Hedrick, 1996; Morbidi et al., 2013), optimal control such as model predictive control (MPC) (e.g., Wang et al., 2014; Gong et al., 2016; Ma et al., 2017; Zhou et al., 2017), and artificial intelligence (AI) based approach (e.g., Gao et al., 2017; Gao and Jiang, 2017). With many different approaches and algorithms to control CAVs, the behavior of CAVs is likely to vary greatly. For example, linear controllers are often concerned with local and string stability through a proper selection of feedback and feedforward gains. Depending on how these gains are selected, acceleration rates implemented can be different. On the other hand, the optimal control approach allows for an explicit formulation of a multi-objective function and constraints. The objective function can include various terms including control efficiency related terms (e.g., deviation from target spacing and relative speed with leader) and comfort related term (e.g., acceleration); and constraints can include finite acceleration/deceleration rates, collision free, etc. Depending on how each term in the objective function is weighted and how constraints are formulated, acceleration/deceleration rates implemented by CAVs can vary. Finally, recent studies suggest that AI based controllers, developed based on cutting-edge machine-learning algorithms, are more adept to tackle complicated driving tasks than the conventional parametric rule-based models (Kuderer et al. 2015; Lefevre et al. 2016; Zhou et al. 2017). Indeed, self-driving vehicles on the road today are typically controlled by some form of "learning-based" data-driven methods. Many different learning algorithms exist, and depending on the algorithms used, the behavior of CAVs can vary.

Most notable studies suggest that the upper/lower bounds of the acceleration rate of CAV should be lower than those of RVs and ideally consistent with those of light rail, at least in the early stage of CAV adoption for driver comfort (Le Vine et al. 2015). Some studies reflect this view by assuming a lower acceleration rate in CAV control (Wang et al. 2014a, 2014b). However, as adoption increases, drivers (or passengers) will become more familiar/comfortable with how CAVs are driven and may accept higher acceleration. Increasing adoption of electric vehicles can expedite the acceptance of a greater range of acceleration/deceleration (Lee and Sul, 1998). Furthermore, as the technology develops, users will be able to customize how CAVs are driven, which can give a rise to highly heterogeneous CAV behavior due to the heterogeneity in human preference (Talebpour et al., 2011). For example, some CAV operation parameters (e.g., desired speed and/or acceleration rates) can be set up by users, including passengers, drivers, or fleet operators, which are likely to result in significant heterogeneity due to the different objectives and driving preference.

In the current work, we investigate (i) how heterogeneity in mixed traffic systems, specifically differences in preferred acceleration rates, desired speeds, and car-following (CF) behavior between RVs and CAVs, manifests itself in transition dynamics as a result of major traffic disturbances (e.g., forced lane changes) and (ii) how the transition dynamics impact mixed traffic throughput. Our *main premise* is that CAVs, depending on their control logic, may

accelerate at higher (or lower) rates than RVs. For instance, CAVs on eco-driving mode would typically be controlled to accelerate more gradually than RVs, and CAVs with control efficiency-oriented logic may allow for sharper accelerations. This systematic difference in accelerations, coupled with differences in desired speeds (between CAVs and RVs and within each group), could seriously undermine traffic throughput, through creation of persistent voids.

Our investigation focuses on how heterogeneity manifests itself in the acceleration (when a vehicle is unconstrained) and CF behavior of vehicles to gain physical insight, rather than tracking all details of the traffic features. Specifically, we first investigate the 'acceleration' behavior influenced mainly by the variation in acceleration capabilities and desired speeds and how that leads to creation of voids (thus throughput reduction). This behavior is studied through analytical modeling and numerical analysis to provide physical insight. The CF behavior is modeled through the "asymmetric behavior" model (AB Model, Chen et al., 2012) and the "chained asymmetric behavior" model (CAB, Srivastava et al., 2018), where heterogeneity manifests in the form of variation in reaction patterns and sensitivity to disturbance magnitude. Finally, we investigate how heterogeneity in CF and acceleration behaviors between RVs and CAVs (and within each) compound throughput reduction by creating additional voids. We examine this compounding effect through an analytical investigation to gain physical insight and numerical simulations to quantify the effect.

The remaining of the paper is organized as follows: Section 2 presents the mechanisms of how acceleration behavior affects traffic dynamics and throughput and Section 3 quantify the impacts on void creation. Section 4 introduces the CF models for RVs and CAVs. Section 5 presents the mechanisms of how CF and acceleration behaviors compound and quantifies the effects. Conclusions and discussions are provided in Section 6.

## 2 Impacts of Acceleration Behavior: Mechanisms

This section investigates the impacts of heterogeneity in acceleration behavior on transition dynamics around a major disturbance and traffic throughput. We first investigate the individual effects of different acceleration rates and desired speed, and then the combined effects. This section will focus on illustrating the mechanisms to provide insight, and the following section will provide the formulations and quantify the effects on throughput.

## 2.1 Impacts of Heterogeneous Acceleration Rates

Heterogeneity in preferred acceleration rates and desired speeds across vehicle classes can cause voids to appear when vehicles emerge from a disturbance. It can also cause vehicle platoons to split or merge as the disturbance propagates, thereby impacting the traffic properties. To illustrate the effect of heterogeneous acceleration rates, we consider two vehicle classes with the same desire speed u but different acceleration rates,  $a_s$  for the smaller rate, and  $a_l$  for the larger rate. As previously mentioned, depending on how CAVs are controlled, CAVs might have a larger or smaller acceleration rate than RVs. To control the compounding effects of CF behavior on void creation (due to time-varying reaction patterns and heterogeneity in them), we assume that vehicles follow Newell's simplified CF model (Newell, 2002) when they are constrained, even during acceleration. More realistic CF behavior will be discussed in Section 4 and integrated in the simulation experiments in Section 5. In Newell's model, a vehicle maintains a constant minimum space,  $\delta$ , and driver response time,  $\tau$ , with respect to its leader along the traffic shock wave when car-following. This means that all states from the leader are passed to the follower along the traffic shockwave (-w): a disturbance will not amplify nor decay.

We examine the LC scenario where vehicles insert into free-flow traffic. We assume that a vehicle inserts into the target lane with initial speed  $v_0 < u$  and accelerates at  $a_{LC}$  till it reaches u as in Laval and Daganzo (2006). This creates a persistent void (i.e., extra time gap) ahead due to the finite acceleration rate (see Fig. 2-1(a)). The void, o, can be derived based on the basic vehicle kinematic characteristics as:

$$o = (u - v_0)^2 / 2ua_{LC} (2-1)$$

Note that Eqn. (2-1) is derived based on the assumption of a constant acceleration rate, which is not realistic since it is well known that acceleration rate is typically a decreasing function of speed. However, dynamic acceleration does not change the main insight of this paper, though the void size would be larger since acceleration will become more constrained as vehicles accelerate. Throughout this paper, we will assume constant accelerations for analytical

investigations to derive physical insights more easily. Dynamic acceleration will be considered later in our simulation experiments to quantify the impact in terms of average void size and throughput reduction.

If the inter-vehicle gap that the LC vehicle inserts into is sufficiently large, the disturbance will be contained in this gap and will not affect subsequent vehicles upstream. Otherwise, the insertion will instigate a disturbance that propagates through vehicles upstream in the platoon. For example, in Fig. 2-1(a), an LC vehicle inserts into a gap  $H = 2h_0$ , where  $h_0$  is the minimum equilibrium time gap in free-flow condition. To accommodate the inserting vehicle without creating a disturbance, the gap should at least equal to  $2h_0 + o$ . Since the gap is not sufficient, the disturbance instigated by the LC propagates to vehicles in platoon  $P_1$ .

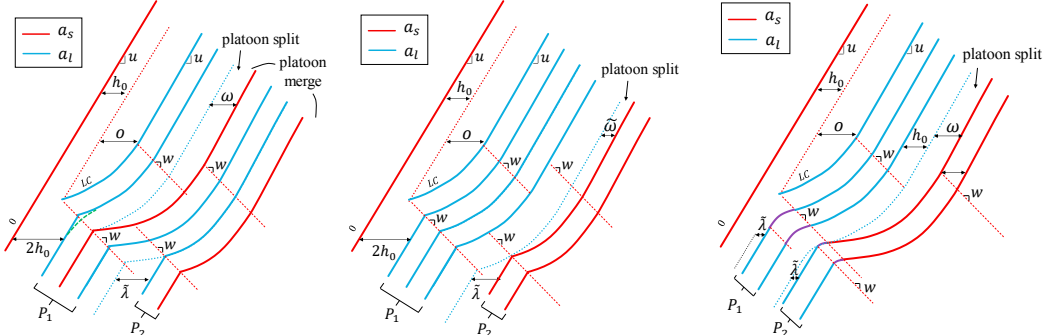


Fig 2-1: Illustration of void creation, disturbance amplification, and platoon merge/split by heterogeneous acceleration: (a) mixed platoons; (b) homogeneous platoons with initial gap  $\tilde{\lambda} = h_0$ ; (c) homogeneous platoon with initial gap  $\tilde{\lambda} < h_0$ ; Red dotted trajectories represent virtual trajectories of the LC vehicles if they inserted at speed u or have infinite acceleration. Blue dotted trajectories represent virtual trajectories if the vehicles were car-following and had the same acceleration rate as the LC vehicle. The trajectories during deceleration are approximated with infinite deceleration in (a) and (b) since this simplifying assumption does not impact the void size. This approximation is illustrated for vehicle 1 in (a); see the green dashed curve.

In the disturbance propagation process, if the LC vehicle has a larger acceleration rate (i.e.,  $a_{LC} = a_l$ ), the disturbance can be amplified when, for the first time, it encounters a vehicle with a smaller acceleration rate  $a_s$ ; see vehicle 2 in Fig. 2-1(a). With the disturbance amplification, an additional void is created, denoted by  $\omega$  given below, causing the platoon to split.

$$\omega = o(a_l/a_s - 1), \tag{2-2}$$

where o is the void given by Eqn. (2-1). Then the total void size,  $o_{tl}$ , increases to:

$$o_{tl} = o + \omega = o(a_l/a_s).$$
 (2-3)

We can see that the total void size,  $o_{tl}$ , increases by a factor,  $\frac{a_l}{a_s} - 1$ . Throughout this paper, this phenomenon will be referred to as the "amplification effect".

As a disturbance propagates upstream, it can be mitigated by an inter-platoon gap,  $\lambda$ , assumed to be greater than  $h_0$ ; see the time gap between platoon  $P_1$  and  $P_2$  in Fig. 2-1 (a). In this case, the two platoons merge and  $o_{tl}$  decreases by the size of extra inter-platoon gap  $\tilde{\lambda}$  (=  $\lambda - h_0$ ).

Note that the platoon composition (mixed vs. homogenous) affects the magnitude of disturbance amplification and thus total void size. Specifically, the platoons in Fig. 2-1(a) are mixed, whereas the platoons in Fig. 2-1(b) are homogenous such that  $P_1$  ( $P_2$ ) consists of vehicles with  $a_l$  ( $a_s$ ) only. In the latter setting, the second void is created between platoons (ahead of  $P_2$ ) but is smaller in size thanks to the absorption by the extra platoon gap,  $\tilde{\lambda}$ . The size of the second void,  $\tilde{\omega}$ , can be derived as below:

$$\widetilde{\omega} = o_{res} \left( a_1 / a_s - 1 \right), \tag{2-4}$$

$$o_{res} = o - \tilde{\lambda},\tag{2-5}$$

where  $o_{res}$  represents the residual void size right before the amplification (given by Eqn. (2-5)), and the second component,  $\frac{a_l}{a_s} - 1$ , represents the amplification factor. Clearly, due to the partial void absorption by  $\tilde{\lambda}$ , the amplification of void size is less than the mixed case. Eqn. (2-4) gives the general formulation for void size amplification, where  $o_{res}$  refers to the void residual, regardless of whether there is void absorption before. The total void size,  $\tilde{o}_{tl}$ , can be given in Eqn. (2-6), which is the general formulation with  $\tilde{\lambda}$  capturing the absorption scale before amplification. Clearly,  $\tilde{o}_{tl}$  decreases with  $\tilde{\lambda}$  and achieves the maximum value when  $\tilde{\lambda}$  is zero. In this case, Eqn. (2-6) converges to Eqn. (2-3).

$$\widetilde{o_{tl}} = o + \widetilde{\omega} = o \frac{a_l}{a_s} - \widetilde{\lambda}(a_l/a_s - 1) = \frac{(u - v_0)^2}{2ua_l} * \frac{a_l}{a_s} - \widetilde{\lambda}(a_l/a_s - 1). \tag{2-6}$$

Note that if LC occurs to a gap  $\lambda < 2h_0$  (i.e.,  $\tilde{\lambda} < h_0$ ), the immediate follower will be forced to decelerate earlier to adapt to the equilibrium position behind the LC vehicle; see Fig. 2-1(c) for an illustration. In this case, there will be a full-scale amplification ( $\omega$ ) when the disturbance reaches  $P_2$ , as the cumulative extra gaps up to  $P_2$  is less than the equilibrium time gap ( $h_0$ ) needed by the LC vehicle. The propagation dynamics will converge to the case in Fig. 2-1(b) after the cumulative extra gap exceeds  $h_0$ .

Depending on the platoon characteristics (vehicle sequence specifically), the disturbance may cause a platoon to split, such as  $P_1$  splitting in Fig. 2-1(a), or a platoon to merge, such as  $P_2$  merging into  $P_1$  also shown in Fix. 2-1(a). We caution that the total void size, given by Eqn. (2-6), is the sum of initial void and an additional void regardless of where the voids occur, because we suppress the CF effect by assuming Newell's CF model. The vehicle sequence will matter in terms of the void size when we consider different CF characteristics (through the AB or CAB model). A more detailed discussion of this will follow in Section 5.

One can see that the nature of additional void creation (and disturbance amplification) is that a vehicle with a smaller acceleration rate does not catch up with its leader that has a larger acceleration rate. Therefore, an additional void will not form if the LC vehicle has a smaller acceleration rate  $a_s$ . In this case, the size of the initial void created upon insertion is at maximum, larger than or equal to  $\widetilde{o}_{tl}$ , and can be obtained from Eqn. (2-1) by setting  $a_{LC} = a_s$ :

$$o^{max} = (u - v_0)^2 / 2ua_s (2-7)$$

## 2.2 Impacts of Free-flow Speed

For the impacts of free-flow speed, we consider two vehicle classes with the same acceleration rate a, but with different desired free-flow speed values,  $u_s$  for smaller speed, and  $u_l$  for larger speed. Similarly, Newell's simplified CF is assumed when vehicles are constrained. Note that we assume that LCs occur in equilibrium traffic, wherein all vehicles travel at  $u_s$ , as vehicles with desired speed  $u_l$  will close any extra gaps and become constrained at  $u_s$ .

There are two possible effects depending on the free-flow speed of the LC vehicle.

- The LC vehicle has  $u_l$ : in this case, the LC vehicle will exceed  $u_s$  as it continues to accelerate and close the void created initially. The LC vehicle will eventually join its leader's platoon and stabilize at  $u_s$ ; see Fig. 2-2 (a). This process is referred to as "void closing". The following vehicles will do the same if they have  $u_l$ , resulting in identical trajectories (e.g., the blue dotted trajectory behind the LC vehicle in Fig. 2-2(a)). This will continue until the disturbance encounters the first vehicle with  $u_s$ , which will only accelerate to  $u_s$  and then cruise at this value. Consequently, the temporary void created by the LC will be shifted to the front of this vehicle and become "permanent"; see Fig. 2-2 (a).
- The LC vehicle has  $u_s$ : in this case, void closing will not occur by the LC vehicle. The upstream following vehicles, regardless of having  $u_s$  or  $u_l$ , will have to stabilize at  $u_s$  as they are constrained by the LC vehicle; see Fig. 2-2(b).

These two cases suggest that a void (either original or additional) might close temporarily, but it will eventually get shifted to the vehicle with smaller free-flow speed. Clearly, the free-flow speed affects the spatial distribution of the voids but not the total void size.

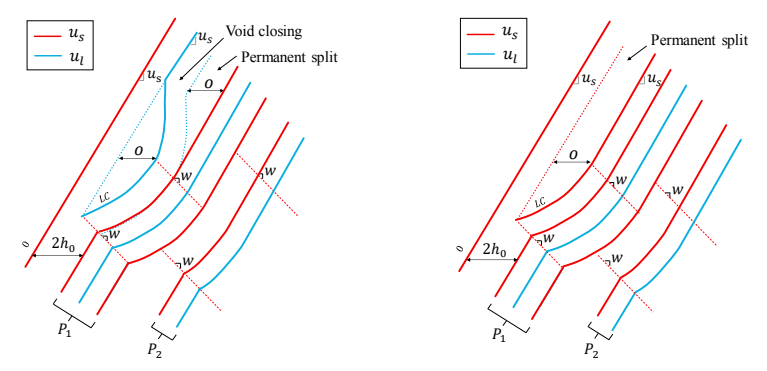


Fig. 2-2: Void creation in platoon: (a) LC vehicle has  $u_l$ ; (b) LC vehicle has  $u_s$ .

### 2.3 Combined Impacts of Acceleration Rate and Free-flow Speed

Here we consider the coupled effects of heterogeneity in acceleration rate and desired free-flow speed. The analysis in the previous subsection suggests that the smaller acceleration rate or free-flow speed imposes a constraint on traffic performance. Specifically, we have learned that (i) along the disturbance propagation path, the first vehicle with a smaller acceleration rate or free-flow speed will be a constraining vehicle that will cause (additional) void creation and disturbance amplification; and (ii) the magnitude of these effects depends on the LC vehicle's acceleration behavior. As such, we examine void creation and disturbance amplification with respect to the LC vehicle's acceleration behavior. There are four combinations based on the two classes of acceleration rate ( $a_{LC}$ ) and two classes of desired free-flow speed ( $u_{LC}$ ) used above:

- Case A  $(a_s, u_s)$ : the LC vehicle has  $a_{LC} = a_s$  and  $u_{LC} = u_s$
- Case B  $(a_s, u_l)$ : the LC vehicle has  $a_{LC} = a_s$  and  $u_{LC} = u_l$
- Case C  $(a_l, u_s)$ : the LC vehicle has  $a_{LC} = a_l$  and  $u_{LC} = u_s$
- Case D  $(a_l, u_l)$ : the LC vehicle has  $a_{LC} = a_l$  and  $u_{LC} = u_l$

Case A  $(a_s, u_s)$ : This is the simplest case as the LC vehicle exhibits the most constraining behavior. The LC vehicle will create a void of maximum size  $o^{max}$  upon insertion, given by Eqn. (2-7). Thus, there is no further amplification by upstream vehicles, and extra gaps upstream will only be used to resolve  $o^{max}$ ; see Fig. 2-3(a).

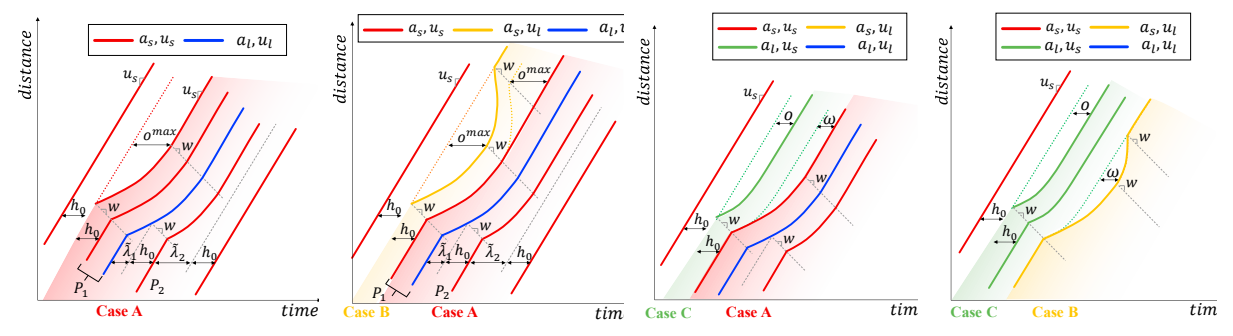


Fig 2-3: Traffic dynamics under Case A, Case B, Case C-1 (FConV has  $(a_s, u_s)$ ), and Case C-2 (FConV has  $(a_s, u_t)$ ).

Case B  $(a_s, u_l)$ : In this case, the LC vehicle has the acceleration constraint  $(a_s)$  but not the desired free-flow speed constraint  $(u_s)$ ; i.e., the acceleration constraint  $(a_s)$  occurs first. The LC vehicle will create a void of maximum size  $(o^{max})$  due to the acceleration constraint but will be able to close it momentarily by exceeding  $u_s$ . The void, however, will re-emerge later ahead of the first constraining vehicle upstream (referred to as FConV) with  $u_s$ ; i.e., the void  $o^{max}$  is shifted. This time, it will persist downstream and thus, reduce the throughput. Notice that in this case, there is no disturbance amplification. Also notice that inter-platoon gaps can diminish the disturbance, but not the void. After the void shift, there is no more disturbance amplification or void shifting, similar to the traffic condition of Case A  $(a_s, u_s)$  right after the insertion; see Fig. 2-3(b).

Case C  $(a_l, u_s)$ : In this case, the LC vehicle has the desired free-flow speed constraint  $(u_s)$  but not the acceleration constraint  $(a_s)$ . Clearly, the LC vehicle will create a smaller void  $(=(u_s-v_0)^2/2ua_l)$ ) due to the larger acceleration rate but will not close it after reaching  $u_s$ . The disturbance may be fully resolved by inter-platoon gaps if there are no constraining vehicles in the propagation path - in this case, there will be no disturbance amplification or additional voids. Otherwise, there will be disturbance amplification and additional void  $(\omega)$  creation. Specifically, there exist two subcases depending on the characteristics of FConV with  $a_s$ . If that vehicle has  $u_s$  (Case C-1), the disturbance amplification causes an additional void that will persist downstream. After the amplification, traffic condition in Case C-1 converges to Case A  $(a_s, u_s)$ ; see Fig. 2-3(c) for the dynamics. In contrast, if that vehicle has  $u_l$  (Case C-2), the additional void is closed momentarily, only to re-emerge ahead of the first vehicle further upstream with  $u_s$ . Thus, the traffic condition upstream of the FConV converges to Case B  $(a_s, u_s)$ ; see Fig. 2-3(d).

Case D  $(a_l, u_l)$ : In this case, the LC vehicle has neither the desired free-flow speed constraint  $(u_s)$  nor the acceleration constraint  $(a_s)$ . The LC vehicle will create a void (in smaller size) but close it momentarily. However, similar to the previous cases, this void will merely be shifted and re-emerge ahead of the next constraining vehicle upstream. Moreover, disturbance amplification and an additional void will occur by a constraining vehicle(s) upstream. Specifically, there exist three potential subcases for traffic evolution, depending on which constraint occurs first in the subsequent vehicles. Note that the traffic evolution behind the LC vehicle has the recursive nature in a sense that depending on the characteristics of the FConV, the traffic evolution will converge to Case A, B or C.

- Case D-1: the FConV has  $a_s$  (i.e.,  $(a_s, u_1)$ ). In this case, the traffic evolution behind the FConV (orange vehicle in Fig. 2-4(a)) converges to Case B in a sense that this FConV will create a temporary additional void that will get shifted later (along with the initial void o) to another vehicle with  $u_s$  upstream; see Fig. 2-4 (a).
- Case D-2: the FConV has  $u_s$  (i.e.,  $(a_l, u_l)$ ). In this case, the initial void, o, appears ahead of the FConV (green vehicle in Fig. 2-4(b)) and then the traffic evolution converges to Case C; see Fig. 2-4 (b).
- Ocase D-3: the FConV has  $a_s$  and  $u_s$ . In this case, the traffic evolution after the FConV converges to Case A: disturbance amplification and an additional persistent void ( $\omega$ ) will occur with the FConV, along with the shifting of the original void (o); see Fig. 2-4 (c).

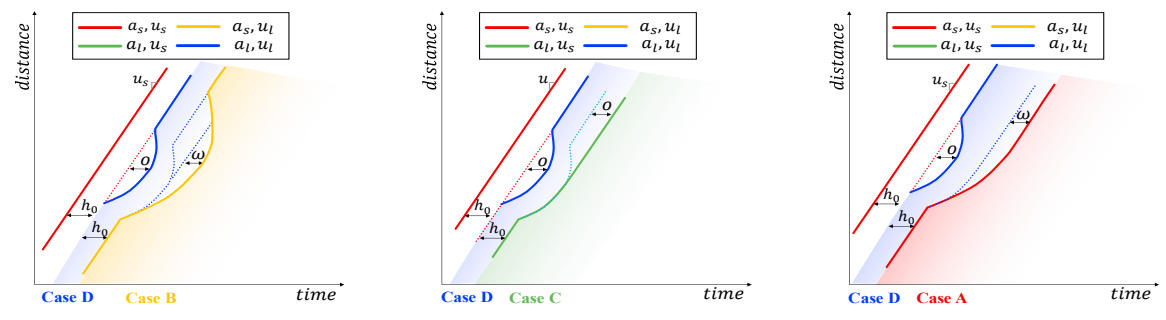


Fig. 2-4: Case D traffic dynamics: (a) Case D-1; (b) Case D-2; (c) Case D-3.

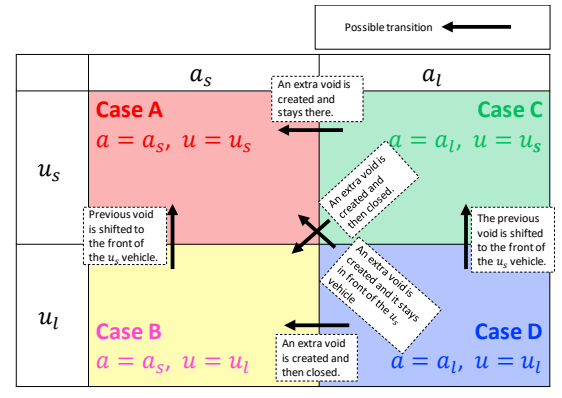


Fig. 2-5: Case transition for the bi-value setting of acceleration rate and desired speed.

Fig. 2-5 illustrates the recursive nature of the traffic evolution, showing the possible case transitions across the four possible cases and the consequence of each transition. This can be viewed in the 2-D plane with four cells. The left column presents the acceleration constraint while the upper row presents the free-flow constraint. Each arrow shows how traffic will evolve from one case to another and the consequent impact on traffic flow when a new constraint emerges. Accordingly, Case D has three different ways of case transition.

#### 2.4 General multi-value case

The previous section focused on the bi-value setting for the acceleration rate a and desired free-flow speed u to understand the impact mechanisms of vehicle heterogeneity on traffic throughput and dynamics. Here we generalize the analysis to a (discrete) multi-valued case; i.e.,  $a = \{a_1, a_2, a_3, ..., a_n\}$ , where  $a_1 < a_2 < a_3 ... < a_n$ , and  $u = \{u_1, u_2, u_3, ..., u_n\}$ , where  $u_1 < u_2 < u_3 ... < u_n$ .

Notably, it turns out that there is no significant difference in traffic dynamics between the bi-valued vs. multi-valued settings of u. Specifically, when a disturbance emerges, a vehicle with  $u_i$  (for  $i = \{2, ..., n\}$ ) will close the void and the void will re-emerge in front of the next upstream vehicle with  $u_1$ . Eventually, all the voids induced by LC will stabilize in front of vehicles with  $u_1$ . The only difference is that if an additional void is very large, a vehicle with a larger free-flow speed can close a void faster. Therefore, the bi-value setting of u provides the key insight into the impact mechanism of heterogeneity in free-flow speed.

In contrast, generalization into multi-valued a is not straightforward, and the bi-valued setting of a does not provide a complete insight. As such, in our following analysis, we consider the n-valued setting for a ( $a = \{a_1, a_2, a_3, ..., a_n\}$ , where  $a_1 < a_2 < a_3 ... < a_n$ ) and bi-valued setting for u ( $u = \{u_s, u_l\}$ , where  $u_s < u_l$ ). Thus, there are 2n combinations, as illustrated in Fig. 2-6, where the rows (columns) indicate the u (a) values. The cases are referred to as Case "Xi" based on the characteristics of the LC vehicle, where "X" indicates the u category, "S" for small and "L" for large, and the number "i" indicates the level of acceleration. Depending on the characteristics of the first constraining vehicle, one case can transition to another. Specifically, we make the following remarks:

- R1: A leftward horizontal transition,  $Si \rightarrow Sj$  or  $Li \rightarrow Lj$  for i > j, represent a downgrade in acceleration. In this case, an additional void will be created, and a disturbance will be amplified. In  $Si \rightarrow Sj$ , the additional void will stabilize and persist downstream; while in  $Li \rightarrow Lj$ , the additional void will be closed momentarily and eventually shifted to another vehicle upstream. Thus, we use horizontal arrows in different colors to distinguish the different post-disturbance dynamics: orange for void stabilizing and yellow for void closing.
- R2: The amplification scale of the void size increases with the acceleration downgrade scale (i.e., the difference between  $a_j$  and  $a_i$ ). The void amplification factor is  $\gamma = a_i/a_j 1$  ( $a_i > a_j$ ). This is straightforward as it is similar to the bi-value case.
- R3: A upward vertical transition,  $Li \rightarrow Si$ , represents a downgrade in desired free-flow speed; see the blue vertical arrow in Fig. 2-6. In this type of transition, there will be void shifting in the post-disturbance process: the previous (temporary) void will be shifted to the front of the next constraining vehicle with  $u_s$  and become permanent.
- R4: A transition can be mixed (i.e. diagonal transition), such as a downgrade in acceleration rate and desired speed (L4→S3) or downgrade in acceleration rate but upgrade in desired speed (S3→L2). Note, however, that an upgrade in acceleration is not possible as acceleration will be constrained by the leading vehicle's acceleration.
- R5: A diagonal transition can be conveniently decomposed into independent horizontal and vertical transitions since the effects of the acceleration rate and the desired speed are independent. For example, in L4→ S3, a disturbance will be amplified, and the cumulative void (the sum of a previous void and an additional void) will stabilize and persist downstream. This is equivalent to L4→ L3 transition (see the dashed yellow horizontal arrow in the figure), which will have the disturbance amplification and void closing, followed by L3→ S3 transition (see dashed blue horizontal arrow), which will have void shifting.

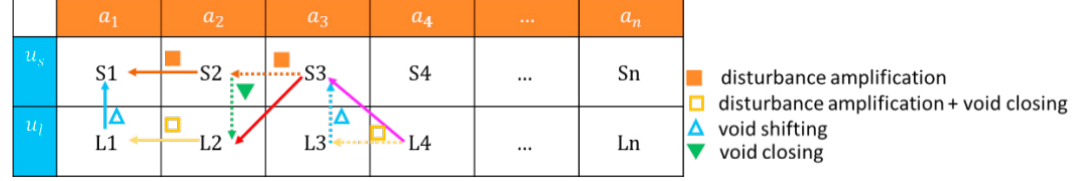


Fig. 2-6: General case transition with the multi-value setting of acceleration rate.

#### 3 Impacts of Acceleration Behavior: Quantification of Void

In this section, we quantify the void creation caused by LCs. We focus on disturbances instigated by a single LC maneuver to derive physical insight. We first provide the formulation of total voids in the bi-valued acceleration setting with homogeneous platoons. Then the formulation for mixed platoons is derived in a similar way. Following that, we also examine the void creation in the n-valued acceleration setting and find similar results with bi-value setting (we omit the results to remain succinct). In our investigation, we assume that all vehicles have the same desired free-flow speed, u, since differences in u do not impact the total void size as shown earlier.

## 3.1 Bi-valued accelerations – homogenous platoons

We consider the bi-valued setting for accelerations  $a = \{a_s, a_l\}$  where  $a_s$  denotes small and  $a_l$  denotes large acceleration rate and  $a_s < a_l$ . Let p denote the penetration rate of  $a_l$  vehicles in the traffic stream. We control for the CF effect by assuming Newell's simplified CF model, consistent with Section 2. We examine the case where platoons are all homogenous; i.e., either all with  $a_s$  (referred to as the  $a_s$  platoon) or  $a_l$  ( $a_l$  platoon). Let  $m_i$  be the platoon size for platoon i and  $\tilde{\lambda}_l$  for the extra platoon gap; see Fig. 3-1. Below, we first simplify the problem by assuming that  $m_i$  and  $\tilde{\lambda}_l$  are both constants, denoted by  $m_s$ , and  $\tilde{\lambda}_s$ , respectively. Such simplification allows us to derive the closed form formulation and obtain insight. Then we examine the case where  $m_i$  and  $\tilde{\lambda}_l$  are randomly distributed and show that the main patterns are similar to the simplified case. With randomly distributed  $m_i$  and  $\tilde{\lambda}_l$ , we resort to simulation as the problem is very complex and intractable in most cases (depending on the distribution).

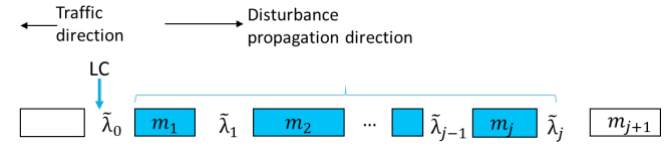


Fig. 3-1: illustration of disturbance propagation extent.

Here we formulate the expectation of the cumulative void size per insertion to throughput reduction. Note that in the bi-value setting the cumulative void has the same meaning with total void size  $(\widetilde{o_{tl}})$  but the cumulative void size is used here to be general as the value is not deterministic and there can be multiple amplification in the n-valued acceleration setting. For an LC, the cumulative void size,  $o_{cum}$ , consists of two parts: the void size of the initial insertion,  $o_{in}$ , and the amplification,  $\widetilde{\omega}$  (within a platoon or across platoons). Thus,  $E[o_{cum}]$  can be expressed as:

$$E[o_{cum}] = E[o_{in}] + E[\widetilde{\omega}] \tag{3-1}$$

The formulation for  $E[o_{in}]$  (based on Eqn. 2-1) is straightforward, as shown below:

$$E[o_{in}] = o_{in,a_l}p + o_{in,a_s}(1-p) = \frac{(u-v_0)^2}{2u} \left(\frac{p}{a_l} + \frac{1-p}{a_s}\right)$$
(3-2)

where  $o_{in,a_l}$   $(=\frac{(u-v_0)^2}{2ua_l})$  is the initial void by an LC with  $a_l$ , and  $o_{in,a_s}$   $(=\frac{(u-v_0)^2}{2ua_s})$  is for LC with  $a_s$ .

Formulation of  $E[\widetilde{\omega}]$ , however, is more complicated as it depends on where the amplification occurs. Since platoon size and inter-platoon gaps are constants, we have the inter-platoon gap  $\widetilde{\lambda}=(1/qh_0-1)h_0m$ , where q is the mainline flow. Let  $\widehat{o}_{a_l}$  (=  $o_{in,a_l}+h_0$ ) denote the initial disturbance in time gap,  $\gamma_{ls}$  (=  $(a_l/a_s-1)$ ) denote the amplification factor, and  $K_1^*(=\lfloor h_0/\widetilde{\lambda} \rfloor)$  and  $K_2^*$  (=  $\lfloor \widehat{o}_{a_l}/\widetilde{\lambda} \rfloor$ ) denote two threshold values -  $K_1^*$  represents the number of extra inter-platoon gaps necessary to provide an additional equilibrium time gap  $(h_0)$  for the LC, and  $K_2^*$  further incorporates the number of extra gaps necessary to absorb  $o_{in}$ . Also let k be the location where the amplification occurs (i.e., at the  $k^{th}$  inter-platoon gap. The formulation of  $\widetilde{\omega}$  is provided below.

$$\widetilde{\omega}|(a_{in}=a_s)=0\tag{3-3}$$

$$\widetilde{\omega}|(a_{in}=a_l) = \begin{cases} C1: & 0, \ w.p. \ p^{K_2^*} \\ C2: \ \gamma_{ls}o_{in,a_l}, \ w.p. \ p^{k-1}(1-p), \forall \ k=1,2,...,K_1^*, if \ K_1^* \ge 1 \\ C3: \ \gamma_{ls}\left(\hat{o}_{a_l}-k\tilde{\lambda}\right), \ w.p. \ p^{k-1}(1-p) \ \forall \ k=K_1^*+1,...,K_2^* \end{cases}$$
(3-4)

C1-C3 correspond to three possible cases of void size amplification. C1 captures the case with no amplification, corresponding to the case where the first  $K_2^*$  platoons are vehicles with  $a_l$ . Since platoons are homogeneous, the probability of encountering an  $a_l$  and  $a_s$  platoon is p and (1-p), respectively. C2 and C3 are cases with amplification. Specifically, C2 is the case for full-scale amplification, in which  $\tilde{\lambda}$  of the initial inserting gap is smaller than  $h_0$  and the immediate follower has to decelerate in advance to reach the equilibrium position behind the LC vehicle (see Fig. 2-1(c) for an example); and the amplification occurs before reaching the  $K_1^* - th$  platoon. If it occurs upstream of the  $K_1^* - th$  platoon (case C3), void size amplification will be partial. Of course, if  $\tilde{\lambda} \geq h_0$  (i.e.,  $K_1^* \geq 1$ ), C2 does not exist. Then  $E[\tilde{\omega}]$  can be found as:

$$E[\widetilde{\omega}] = pE[\widetilde{\omega}|a_{in} = a_i] + (1 - p)E[\widetilde{\omega}|a_{in} = a_s]. \tag{3-5}$$

We omit the elaborate form for  $E[o_{cum}]$  to remain succinct. Fig. 3-2(a) illustrates the results of  $E[o_{cum}]$  and its two sub components with respect to platoon size m under the same mainline flow  $q=0.8/h_0$ . Note that the size of extra gap,  $\tilde{\lambda}$ , is linearly proportional to m; i.e., if platoons are longer, the inter-platoon gap will be larger, though the frequency is lower. From the figure, one can see that  $E[o_{in}]$  remains constant, as expected, but the amplification component decreases with platoon size. This is because with longer platoons, the size of extra gaps will be larger and thus the gaps absorb the disturbance earlier. Note that  $E[\tilde{\omega}]$  becomes zero (and  $E[o_{cum}]$  remains constant) after m exceeds a threshold, because when  $\tilde{\lambda}$  is sufficiently large, the disturbance will be fully resolved by the first insertion gap and there is no amplification. One can also see that  $E[o_{in}]$  decreases as p increases. This is intuitive because when the proportion of  $a_l$  increases, the proportion of the smaller initial void,  $o_{in,a_l}$ , is larger.

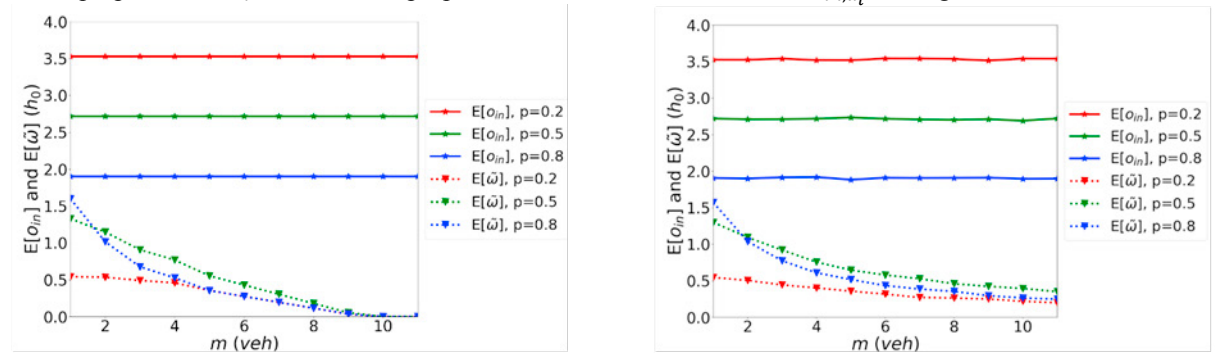


Fig. 3-2:  $E[o_{cumu}]$  with homogeneous platoons: (a) deterministic constant  $m_i$  and  $\tilde{\lambda}_i$ ; (b) randomly distributed  $m_i$  and  $\tilde{\lambda}_i$ .

We also conduct simulations to examine randomly distributed  $m_i$  and  $\widetilde{\lambda}_i$ , where  $m_i$  follows a discrete uniform distribution  $\sim U(1, 2m-1)$ , and  $\widetilde{\lambda}_i$  follows an exponential distribution  $\sim Exp(\widetilde{\lambda})$ . Note that the expected values for  $m_i$  and  $\widetilde{\lambda}_i$  are the same as the deterministic case. Fig. 3-2(b) shows the results. One can see that after adding the randomness,  $E[o_{in}]$  is not affected, but  $E[\widetilde{\omega}]$  decreases much more slowly and does not converges 0. This is because there are always chances that the void would be amplified, as long as the sum of first m extra gaps is smaller than  $o_{in}$ . Overall, the main patterns of the plots in Fig. 3-2(b) are similar to the deterministic case in Fig. 3-2(a), suggesting that the deterministic case has captured the key features of throughput.

### 3.2 Bi-valued accelerations – mixed platoons

Here we consider a similar setting in Section 3.1 but platoons are mixed instead of homogeneous. For mixed platoons, the formulations for  $o_{in}$  (given by Eqn. (3-2)) and  $\widetilde{\omega}|(a_{in}=a_s)$  in the homogeneous case still hold. The formulation for  $\widetilde{\omega}|(a_{in}=a_l)$  follows a similar principle but the probabilities for the different cases vary; see below.

$$\widetilde{\omega}|(a_{in}=a_{l}) = \begin{cases} C1: & 0, & w.p. \ p^{mK_{2}^{*}} \\ C2: & \gamma_{ls}o_{in,a_{l}}, \ w.p. \ p^{m(k-1)}(1-p^{m}) \ for \ k=1,2,...,K_{1}^{*}, \\ & if \ K_{1}^{*} \geq 1; or \ w.p. \ 0, if K_{1}^{*} < 1 \\ C3: & \gamma_{ls}\left(\hat{o}_{a_{l}}-k\tilde{\lambda}\right), \\ & w.p. \ p^{m(k-1)}(1-p^{m}) \ for \ k=K_{1}^{*}+1, K_{1}^{*}+2,...,K_{2}^{*} \end{cases}$$

$$(3-6)$$

where the probability of C1 is  $p^{mK_2^*}$  because now the two vehicle types randomly distribute in platoons and C1 will occur only if the disturbance encounters  $K_2^*$  platoons that are purely  $a_l$  vehicles. C2 and C3 require that the first (k-1) platoons are all  $a_l$  vehicles and there is at least one  $a_s$  vehicle in platoon k.

The expected values,  $E[\widetilde{\omega}]$  and  $E[o_{cum}]$ , can be obtained by plugging Eqn. (3-6) into Eqn. (3-5) and Eqn. (3-1), respectively. We omit the elaborate forms but illustrate the results through figures. As expected,  $E[\widetilde{\omega}]$  decreases with m and p, similar to the patterns in the homogeneous case; see Fig. 3-3(a). Fig. 3-3(b) compares  $E[o_{cum}]$  between the homogeneous (solid lines) and mixed (dashed lines) cases. Note that the difference is purely attributed to  $E[\widetilde{\omega}]$  as  $E[o_{in}]$  is the same in both setting. One can see that in the mixed case,  $E[\widetilde{\omega}]$  is larger and the difference increases with p, which is expected because with larger p the probability of no amplification (C1) is much smaller (i.e., more likely for amplification to occur). Moreover,  $E[\widetilde{\omega}]$  decreases much slowly when m is small. This is because when m is small (the extra gaps are small too),  $K_1^*$  will be large and the contribution of C2 to  $E[\widetilde{\omega}]$  is very significant. In such case, there will be always a full-scale amplification as long as there exists one or more  $a_s$  vehicle among the  $K_1^*$  platoons. Note that the vehicle number in the  $K_1^*$  platoons is  $mK_1^*$ , which only varies slightly with m (due to the floor function). Thus, the contribution of C2 to  $E[\widetilde{\omega}]$  is similar across different m.

Like the homogeneous case, we conduct simulations where  $m_i$  and  $\tilde{\lambda}_i$  respectively have the same distribution setting with the homogeneous case. It was found that the results show similar patterns with the deterministic case. We omit that to remain succinct.

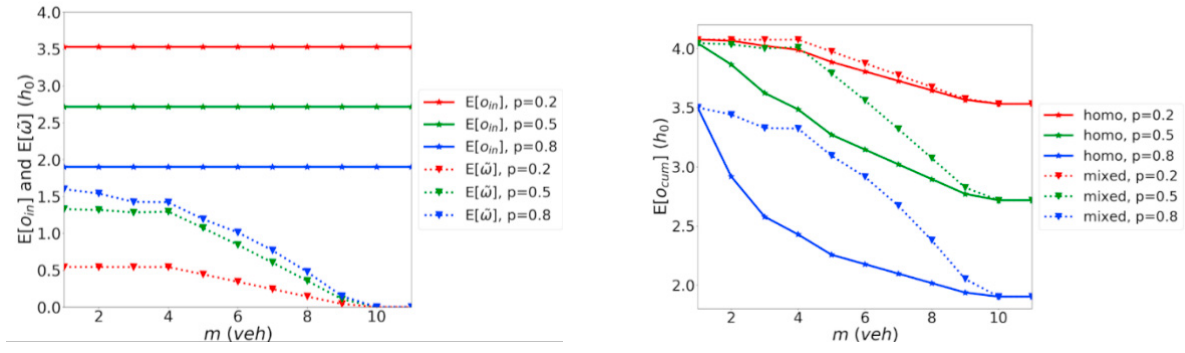


Fig. 3-3:  $E[o_{cumu}]$ : (a) mixed platoons; (b) comparison of homogeneous and mixed platoons.

## 4 Car Following Behavior

This section will examine the CF behavior of RVs and CAVs that can compound the effects of acceleration behavior on the void size amplification and thus, throughput reduction. Two aspects of CF behavior are discussed: one related to the time-varying aspect of driver or vehicle reaction patterns to a disturbance and one related to the systematic differences in reaction patterns between RVs and CAVs. To facilitate this discussion, we first summarize the CF models relevant to this study.

#### 4.1 Car-Following Models - Background

Dating back to the 1950s, CF models have been developed using various guiding principles, such as collision avoidance (Pipes, 1953; Gipps, 1981), stimulus-response models (Newell, 2002; Bando et al., 1995; Kesting et al., 2010), psychological models (Michaels, 1963; Wiedemann, 1974; Saad et al., 1994), as well as artificial intelligence (AI)-based models in more recent times (Kikuchi and Chakroborty, 1992; McDonald et al., 1997; Hongfei, 2003; Panwai and Dia, 2007),. The reader is referred to (Brackstone and McDonald, 1999; and Aghabayk et al., 2015) for

an extensive review of various CF models. While psychophysical and AI models offer interesting insights, the present study relies on CF models based on understanding of the physics of traffic, like the ones in the former categories. To study the effect of CF behavior on void size amplification, we use the AB and CAB models, because they provide a basic model structure consistent with Newell's CF model to further investigate vehicle heterogeneity manifested in CF behavior. While the models simplify certain complexities of vehicle behavior in small time scales, they provide a simple tractable foundation to studying the overall evolutionary pattern of traffic and drawing insights analytically. The AB and CAB models further provide flexible, unified frameworks to capture heterogeneity in the CF behavior of RVs as well as CAVs. Note that other well-known CF models, e.g., Intelligent Driver Model (Kesting et al., 2010), could also be used to investigate the issue of throughput reduction due to heterogeneity in vehicle characteristics. However, such investigation would resort to simulations as it would be difficult to decompose the mechanisms into different elements by controlling for the CF behavior, as we have done in the present study to shed light on various mechanisms of throughput reduction and their interactions.

Below, we summarize the CF models used in our study, starting with an introduction to Newell's CF model. Newell's Simplified Model

Newell (2002) provided a simplified CF model based on the principal that a vehicle maintains a constant minimum space,  $\delta$ , and time gap (driver response time),  $\tau$ , with respect to its leader along the traffic shock wave. Under congested conditions, this means that all states from the leader are passed to the follower along the traffic shockwave (-w).

$$x_i(t) = x_{i-1}(t-\tau) - \delta. \tag{4-1}$$

## AB Model

The AB model (Chen et al 2012a) used a variable,  $\eta(t)$ , to capture a vehicle's deviation from its equilibrium position (defined by Newell's simplified CF model) over time; see Eqn. (4-2) where  $x_i(t)$  and  $x_{i-1}(t)$  are the position of vehicle i and its leader i-1, respectively. Thus, the evolution of  $\eta(t)$  reveals the driver's CF driving characteristics. It was found that when vehicles (RVs) experience a disturbance,  $\eta(t)$  exhibited several shapes, named the "reaction pattern", including concave and convex reaction patterns (see Fig. 4-1 for an illustration).

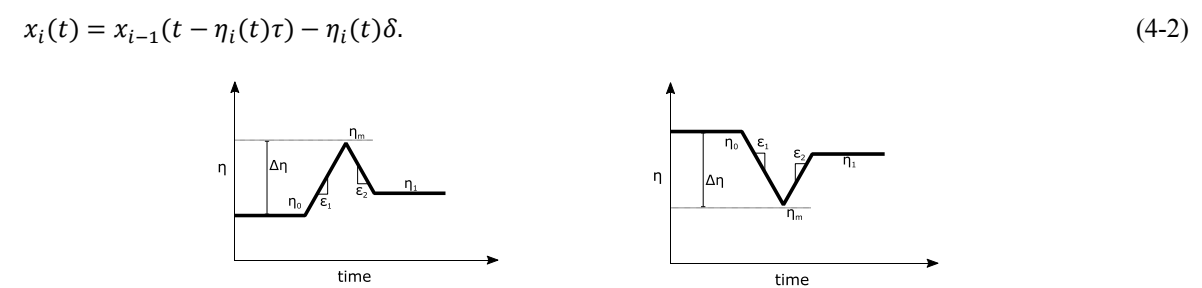


Fig. 4-1: Driver reaction patterns under disturbance: concave (left) and convex patterns (right).

#### CAB Model

Drawing on the AB model, Srivastava et al., (2019) proposed the CAB model based on the observation that the magnitude of change in reaction,  $\Delta \eta = |\eta_m - \eta_0|$  (where  $\eta_0$  is the initial and  $\eta_m$  is the maximum/minimum value of  $\eta$  as a vehicle navigates through a disturbance), varies with the leader's speed variation and deceleration rates, so that a vehicle has a greater deviation in  $\eta$  if its leader exhibits a larger speed reduction; see Eqn. (4-3), where  $v^{init}$  and  $v^{min}$  are a vehicle's initial and minimum speeds during an oscillation and f(.) is a function quantifying the correlation. While Newell's simplified model suggests that the leader's behavior does not affect  $\tau$  and  $\delta$  (thus constant), the AB model extends it to suggest that it affects the follower's response, resulting in time-varying  $\tau$  and  $\delta$  captured by  $\eta(t)$ . The CAB model further extends it by capturing the second-order effect that the follower's response depends on the magnitude of disturbance observed in the leader. While we prefer a parsimonious model in describing key traffic features, it turns out that this second-order effect significantly impacts throughput as we will show in Section 5. Therefore, we use the CAB model, albeit at the expense of increased complexity.

$$\Delta \eta_i = |\eta_m - \eta_0| = f(v_{i-1}^{init} - v_{i-1}^{min}) \tag{4-3}$$

#### 4.2 Modeling CF behavior

This section establishes a unified framework to model CF behavior of RVs as well as CAVs through the AB and CAB (C/AB hereafter) models. This unified framework enables us to investigate the compound effects of heterogeneous acceleration and CF behaviors analytically as well as using simulations.

Heterogeneity within RVs' CF behavior stems from individual drivers responding uniquely to their leader's driving. In mixed traffic conditions, the presence of CAVs further adds to the heterogeneity: while CAV behavior will have less stochasticity attributed to human behavior, CAVs are likely controlled for different objectives or to follow different logic, leading to different CF behaviors across CAV types and from RVs. The varying CF behaviors in mixed traffic can impact the disturbance propagation and throughput. Here we consider CAV control with two major themes: (a) CAVs controlled with emphasis on control efficiency, allowing for larger acceleration/deceleration rates, referred to as the control efficiency-oriented vehicles (CEVs); and (b) CAVs controlled for smoother, eco-driving for fuel efficiency and emission, favoring smaller speed variation, referred to as smooth driving-oriented vehicles (SDVs). SDV control is attractive from the perspective of passenger's comfort and energy efficiency, while CEV control might be desirable in situations where vehicles have deviated from their equilibrium spacing (e.g., due to leader's deceleration), so that they can resume safe spacing as soon as possible and maintain string stability.

In this work, we calibrate both the AB and CAB models to approximate the CF behavior of CAVs traveling through disturbances, in addition to RVs. This will allow us to model both RVs and CAVs in simple yet flexible, unifying frameworks (AB and CAB frameworks) and enable analytical investigations. The use of the C/AB models is even more appealing for AI-based controllers as they are designed to emulate human driving behavior. In this study, we use the state-of-the-art CAV control model by Zhou et al. (2017) as an example to illustrate the proposed approximation by the C/AB models and demonstrate systematic differences in CF behavior between RVs and CAVs.

We used the Zhou et al. (2017) model to generate representative trajectories for a CEV and an SDV platoon, respectively, as they follow a leader undergoing stop-and-go disturbances. The leader's trajectory is artificially synthesized to represent a variety of disturbances (varying initial speeds, speed reductions, acceleration and deceleration rates). The (Zhou et. al. 2017) model, based on a linear quadratic regulator (LQR) optimization, produces closed-form results for CAV trajectories with an ability to incorporate user-defined control objectives, offering an attractive way to simulate both CEV and SDV behavior. The setup used for this paper incorporated three objectives for the controller: (i) minimize deviation from equilibrium spacing, (ii) minimize speed difference with the immediate leader, and (iii) minimize acceleration rate for the CAV follower. The relative priority for the objectives were varied to simulate CEV (prioritizing the former two objectives) and SDV (prioritizing lower acceleration) CF behavior.

The trajectories generated for each scenario (various leader trajectories, each with an SDV and a CEV platoon) are then used to calibrate the response of SDVs and CEVs in the C/AB models. This is done through a two-step process. First the trajectories are used to compare the following distances for a vehicle compared to its leader along the shockwave. The following distances are then used to compute the  $\eta(t)$  profile for each vehicle (since time gap is  $\eta * \tau$ ), as the method used in Chen et al. (2012). Fig. 4-2 shows an example of the simulated CAV trajectories based on the Zhou et al. model, speed profiles, and  $\eta(t)$  for CEVs and SDVs. It is important to note that the control objective for SDVs does not guarantee string stability of the system (i.e., the minimum speeds of vehicles in platoon decreases upstream); see Fig. 4-2(d). In contrast, the CEV platoon is string-stable and the oscillation amplitude (i.e., speed reduction) decreases upstream; see Fig. 4-2(c). We can also see that CEVs opt for lower overall change in  $\eta$ , while SDVs delay a change in speed as late as possible but later they result in lower speed. Clearly, there are distinguishable differences in the reaction patterns of the two types, although they both exhibit a (approximately) convex reaction pattern overall (see Fig. 4-2(e-f)), in contrast to RVs that exhibit a variety of reaction patterns.

For AB model calibration, the  $\eta(t)$  computed over all CEVs (or SDVs) is aggregated to determine an average reaction pattern in response to disturbance regardless of the leader's speed reduction magnitude. For the CAB model calibration, we explore the relation between the follower's reaction change magnitude ( $\Delta \eta = |\eta_m - \eta_0|$ ) with respect to the leader's speed reduction across the disturbance ( $\Delta v$ ). Fig. 4-3 suggests that (1) there is a clear positive correlation between  $\Delta \eta$  and  $\Delta v$ , for both CEVs and SDVs, and (2) SDVs have stronger changes in reaction (higher  $\Delta \eta$ ) than CEVs (see the different slopes of the regression lines with coefficient 0.012 vs. 0.017). (Note that the difference in slope as well as the slopes themselves are all statistically different with the p-values less than 5.5E-5.)

The result in (1) is similar to the results of RVs based on empirical data (Srivastava et. al., 2019), confirming that the CF behavior of CAVs (specifically CEVs and SDVs) can be captured by the CAB framework. More importantly, now we can unify RVs and CAVs through the same frameworks, the AB model and/or the CAB model.

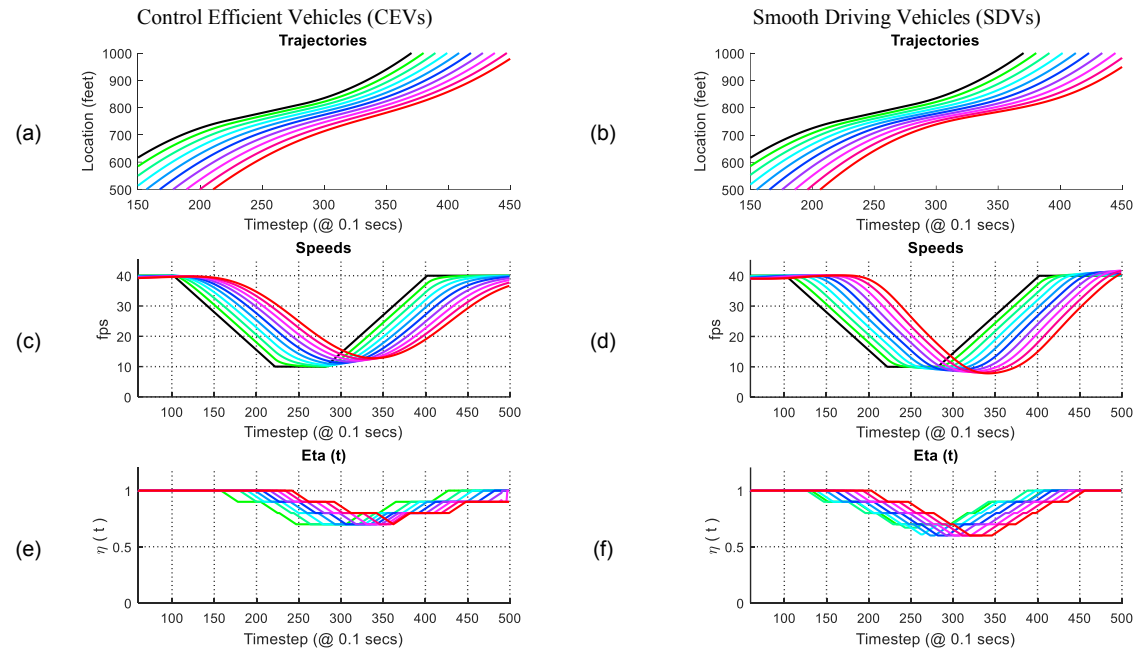


Fig. 4-2: CAV behavior for CEV (left) and SDV (right) controls, showing vehicle trajectories (top), speeds (middle) and driving behavior  $\eta(t)$  (bottom) for a platoon of CAVs.

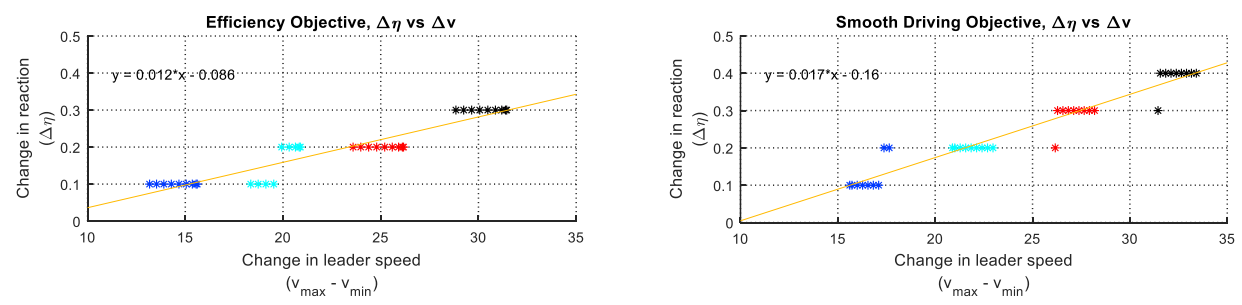


Fig. 4-3: Reaction sensitivity for CAVs: (a) CEVs, (b) SDVs; Each data point represents reaction of a single vehicle in a CAV platoon. Each color block represents response for a platoon of CAVs to a given disturbance in leader trajectory. The graphs represent responses generated for 10 vehicle platoons following 4 varied leader trajectories. Note that the results presented in Fig. 4-2 correspond to the black cluster here.

In summary, we first generate vehicle trajectories of the two CAV types (CEVs and SDVs), measure the  $\eta(t)$  profiles, and then approximate the  $\eta(t)$  profiles into both the AB and CAB frameworks (e.g., extracting the  $\eta_0$  and  $\eta_m$  values and the shape of  $\eta(t)$ ). Note that approximation is done using both the AB and CAB frameworks so that we can compare their performance. The calibration process is identical to that used for calibrating RVs.

## 5 Combined effects of acceleration and car-following

In Sections 2, we set up the basic ideas for how acceleration heterogeneity affects dynamics of a platoon using analytical modeling techniques, while simplifying the car-following aspect through usage of Newell's simplified model. This setup was expanded in Section 3 to a more generalized scenario with demand-dependent platoon structures. In this section, we first illustrate the compounding effects of CF and acceleration behavior and then examine

their impacts on traffic throughput. To unveil the key mechanisms, we first limit ourselves to just a pair of vehicles for an analytical investigation (Section 5.1), where we use a constant acceleration model with the AB car-following model. The more complex case of a scaled up multiple vehicle setup with varied combinations of acceleration and car-following models is investigated using simulations in Section 5.2 as this is not analytically tractable.

#### 5.1 Mechanisms

Below we illustrate some mechanisms of void creations due to the combined effects of car-following and finite acceleration. Notably, deceleration behavior in car-following can contribute to void creation and thus, will be examined in detail. Specifically, we will illustrate that certain car-following behavior, i.e.,  $\eta$  evolution, during deceleration, can limit the vehicle's capability to catch up with the lead vehicle during subsequent acceleration and thus result in void creation. To see this, we examine a simple case with a pair of vehicles, where the leader decelerates from free-flow speed u (30m/s) to a minimum speed  $v_{lead}^{min}$  (15m/s) at a constant rate  $d_{lead}$  (2m/s<sup>2</sup>) and then resumes u at a maximum constant rate  $a_{lead}$  (2m/s<sup>2</sup>). Then, we examine the different cases of response from the immediate follower.

First, we control the acceleration behavior (across different cases for the immediate follower) to study the impacts of different reaction patterns during the deceleration process. For the immediate follower, we examine two cases of deceleration rate: Case 1 with a larger deceleration rate  $d_1$  and Case 2 with a smaller rate  $d_2$ ; i.e.,  $d_2 < d_1 < d_{lead}$ . After reaching the minimum speed  $v_{lead}^{min}$ , the immediate follower accelerates at the same maximum rate of  $a_{lead}$ ; see Fig. 5-1 for the resulting reaction patterns, speed profiles, and vehicle trajectories for the two cases. Both cases result in approximately convex reaction patterns but with different features (Fig. 5-1(a)). (Admittedly, the reaction pattern is not strictly convex for either case; however, the general shape of upside-down triangle is consistent with the convex pattern assumed in the C/AB models.) In Case 1 (with  $d_1$ ), the follower's reaction is characterized by a smaller  $\epsilon_1$ (the change rate of  $\eta$ ) and  $\Delta \eta$  (the change magnitude) compared to Case 2. Notice that the  $\eta$  evolution in deceleration process affects the  $\eta$  evolution in the subsequent acceleration process because the acceleration is finite: the follower in Case 2 cannot display a smaller  $\epsilon_2$  as that requires stronger acceleration than  $a_{lead}$ . Eventually, both cases create voids, but the void size is greater for Case 2 (  $o = (\eta_1 - 1)h_0 = 0.11h_0$  for Case 1, as opposed to  $o = 0.42h_0$  for Case 2). Note that if the follower behaves according to Newell's model, there would be no void. Thus, the difference in the void size  $(0.11h_0)$  vs.  $0.42h_0$ ) results from the combined effects of different reaction patterns (specifically the deceleration process) and the finite (but homogenous) acceleration. The result suggests that the finite acceleration, though homogenous among vehicles, can contribute to void creation when it is compounded with certain reaction patterns in the deceleration process of CF.

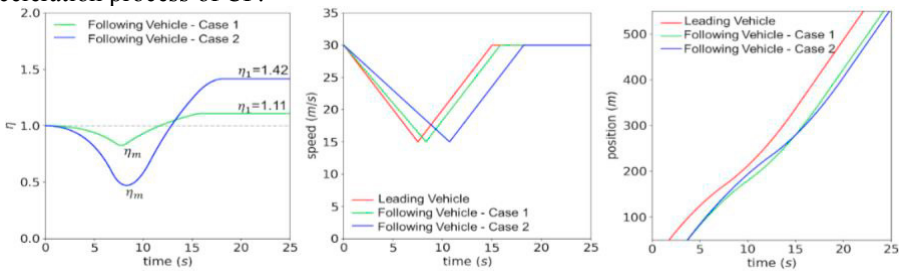


Fig. 5-1: Impacts of different reaction patterns on void creation ( $d_{lead} = 2m/s^2$ ,  $d_1 = 1.8m/s^2$ ,  $d_2 = 1.4m/s^2$ ):  $\eta - t$  plot (left), v - t plot (middle); and x - t plot (right).

Next, we control the deceleration process to study the impacts of heterogeneous acceleration capability. For the follower, we consider three cases of acceleration rate:  $a_1 > a_{lead}$  (Case 1),  $a_2 < a_{lead}$  (Case 2), and  $a_3 = a_{lead}$  (Case 3), where  $(a_1 + a_2)/2 = a_3$ . Also, the follower in all the three cases decelerates to  $v_{lead}^{min}$  at a rate  $d_{follower} = 1.5m/s^2$ . From the resulting  $\eta$  evolution, one can see that all three cases lead to a void. Moreover, the average void size between Case 1 ( $o = (\eta_1 - 1)h_0 = 0.21h_0$ ) and Case 2 ( $o = 0.46h_0$ ) is  $0.335h_0$ , larger than the void for Case 3 ( $o = 0.32h_0$ ), suggesting that heterogeneous accelerations result in larger cumulative voids. Note that the difference in the void size across the three cases is the effect of heterogeneous and finite accelerations.

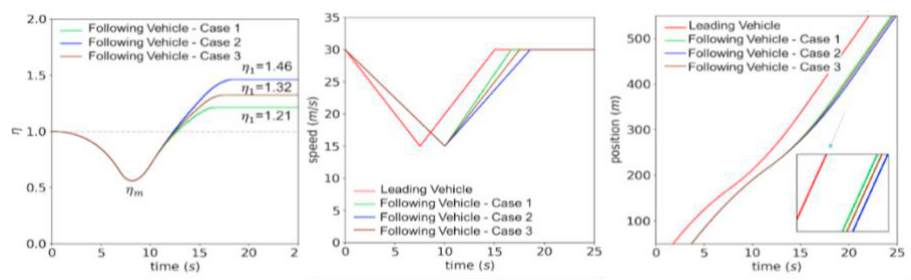


Fig. 5-2: Impacts of heterogeneous acceleration (with deceleration process controlled)  $(d_1 = d_2 = 1.5m/s^2, a_{lead} = 2m/s^2, a_1 = 2.25m/s^2, a_2 = 1.75m/s^2, a_3 = 2m/s^2)$ :  $\eta - t$  plot (left), v - t plot (middle); and x - t plot (right).

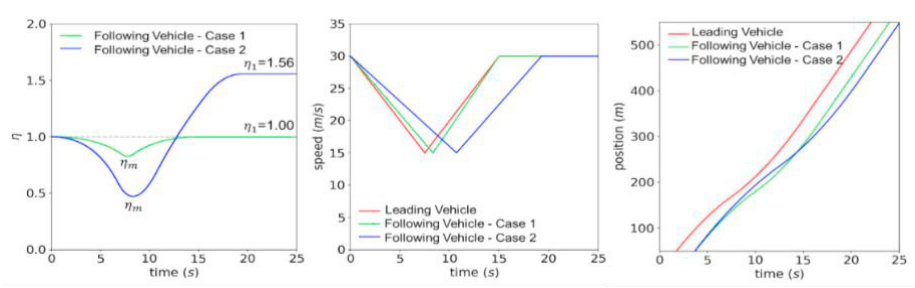


Fig. 5-3: Compound impacts of deceleration and acceleration  $(a_1 = 2.25m/s^2, a_2 = 1.75m/s^2, d_1 = 1.8m/s^2, d_2 = 1.4m/s^2)$ :  $\eta - t$  plot (left), v - t plot (middle); and x - t plot (right).

Below, we study the compounding effects of heterogeneous deceleration and acceleration behaviors. Specifically, we examine two cases for the follower: Case 1 has larger acceleration and deceleration rates,  $(d_1, a_1)$ , than Case 2 with  $(d_2, a_2)$ ; i.e.,  $d_2 < d_1 < d_{lead}$ , and  $a_2 < a_{lead} < a_1$ ; see Fig. 5-3. In both cases, the follower decelerates to  $v_{lead}^{min}$  and then accelerate to resume u. One can see that with the two behaviors compounded, no void is created for Case 1  $(\eta_1 = 1)$  while Case 2 creates a large void  $(o = 0.56h_0)$ . The difference in the void size is larger than the individual effect. Note that, the reaction patterns of Case 1 and 2 represent typical expected patterns for CEV (with smaller  $\eta$  changing rate and smaller  $\Delta \eta$ ; see Fig. 4-1 (e)) and SDV (with larger  $\eta$  changing rate and larger  $\Delta \eta$ ; see Fig. 4-1 (f)), respectively.

The cases illustrated above are all related to convex reaction patterns, but the main conclusions apply to concave reaction patterns. We omit the analysis of concave reaction patterns to keep the paper succinct.

## 5.2 Compound Effect through Multiple Vehicles: Simulations

For a platoon of following vehicles in a fully connected environment, the CF properties for each vehicle (RV or CAV, type of control if CAV, reaction pattern, reaction sensitivity), as well as their acceleration properties (preferred acceleration rate and desired speed) may be known in advance. In such scenarios, the propagation of a given disturbance can be computed from modeling the CF trajectory of each vehicle in the platoon individually from the CAB model (Eqn. (4-3) above), using simulation tools.

We perform three simulation experiments to compare the impacts of (i) homogenous vs. heterogeneous acceleration rates, (ii) Newell's CF model, AB model, vs. CAB model, and (iii) constant vs. dynamic acceleration on void creation and throughput, each with mixed traffic stream consisting of both RVs and CAVs. Each experiment involves simulating the behavior of a 10-vehicle platoon (including a leader that is immediately following an LC vehicle and reacts with a sudden (but smooth) deceleration upon insertion, followed by a gradual recovery acceleration). Each follower in the platoon may switch between acceleration (constrained by its desired acceleration rate), cruise control (constrained by its desired speed), and CF (constrained by the reaction pattern  $\eta(t)$  and deceleration rate) modes. The constraining behavior for a follower is computed at each simulation time step. An additional external constraint further ensures that vehicles do not experience negative speeds. Since the CF behavior reaction pattern never falls below a threshold  $\eta_t$  value ( $\eta \ge \eta_t > 0$ ), the model intrinsically ensures a collision free simulation. Where either the AB or CAB model are used, vehicle CF behavior (e.g., RV or CAV, type of control if CAV, reaction pattern, reaction sensitivity) stochastically drawn from a sample that represents overall distribution for the traffic stream (for RVs, the

sample is taken from measurement of NGSIM data as in Chen et al. 2012; for CAVs, the sample is from trajectories generated by the LQR controller of Zhou et al. (2017)).

In the first experiment, simulations were run to cover a variety of randomly generated scenarios with various combinations of control parameters: CAV penetration rates, acceleration rate distribution, and CF reaction patterns. The CF behavior of the vehicles is described by the CAB model for both vehicle types. For the acceleration behavior (preferred acceleration rate and desired speed), we use a constant acceleration model where acceleration is a constant value. Each vehicle is assigned vehicle type (RV or CAV) drawn from a CAV penetration rate. Similarly, each vehicle is further assigned acceleration and desired speed properties in a similar fashion, drawn from a predetermined range representing typical traffic behavior. The desired speeds and the accelerations are either homogenous (across all vehicles in the platoon), or heterogenous (randomly drawn from a range of values). Each simulation was monitored for the resulting platoon trajectories generated, as well as the minimum speeds within the platoon (the extent to which speed reduction amplifies), and the total throughput (or the extra voids created).

Table 5-1 Total void created (as a multiple of  $h_0$ ) in a platoon of 10 followers under different follower CAV penetration rates, comparing scenario with vehicles exhibiting homogenous and heterogenous distribution of desired acceleration rate.

	Homogenous Acc.	Heterogenous Acc.
20% CAV Setup	2.82	4.24
50% CAV Setup	2.31	4.12
80% CAV Setup	2.07	3.08

Table 5-1 shows a representative summary of cumulative 'voids' (normalized by  $h_0$ ) obtained from the simulations across the 10-vehicle platoon against the CAV penetration rate and acceleration heterogeneity. The table reports result from specific platoon setups randomly generated for each corresponding CAV penetration rate but held consistent between scenarios exploring homogenous and heterogenous acceleration rates. Therefore, the values across the columns in each row represent the impact of acceleration heterogeneity with all other factors (platoon composition, ordering, and CF reaction patterns, speed heterogeneity etc.) controlled. The table illustrates two main findings from the experiment. First, we can draw that CAV penetration rate has a noticeable impact on the cumulative void size generated. Since the platoon composition directly impacts the CF reaction patterns, as well as potentially the acceleration properties, it is not surprising that CAV penetration rate would impact the void size. In addition, the table suggests that void sizes tend to decrease as more CAVs are introduced into the platoon. However, due to the complexity in both enumerating all possible combinations of platoon ordering for a detailed comparison, as well as the substantial impact the ordering would have on the void size, we cannot reliably state that there is a linear relationship exhibited between CAV penetration rate and cumulative void size. A second observation from the table is that acceleration heterogeneity adversely impacts the void size with consistently smaller void sizes observed for scenarios with homogenous acceleration. This second observation is consistent with findings in Section 2. The aggregated results from the full experiment, which consisted of a total of 100 simulations run with varying CAV penetration rates each for scenario with homogenous and with heterogenous acceleration further supported this finding, showing a statistically significant impact of heterogeneity in acceleration behavior (hypothesis that a binary identifier for homogenous or heterogenous acceleration has no impact on void size rejected with a p value < 0.001).

For the second experiment, we used a similar setup as above, except that we now use three CF models: Newell's simplified CF model, AB model, and CAB model, to compare their performance. Each model consisted of trajectories for a ten-vehicle platoon reacting to a disturbance experienced by the leader. The trajectory for each vehicle is computed from a combination of the CF behavior, acceleration behavior (with heterogenous rate), and finite deceleration regardless of the CF model being used. The vehicles are randomly assigned a vehicle type and correspondingly CF features - RVs will have concave reaction patterns and CAVs have convex reaction vehicles for the AB and CAB setups. Note that the choice to only use concave reactions for RVs was made here strictly for simplicity of illustration of results so that RVs and CAVs are easily distinguishable. The simulation could easily be adjusted to allow convex reaction RVs as well. Vehicles are also assigned either a low  $(1.22 \ m/s^2)$  or a high  $(1.52 \ m/s^2)$  desired acceleration value to represent heterogeneity. Since Newell's family of models allow instantaneous deceleration rates, the vehicle speeds are smoothened using a moving window average over 1 second. This smoothening process may impact the void creation and the throughput in combination with the CF behavior, but allows for a more practically meaningful modeling. For the purpose of the experiments presented below, the platoons were

homogenous with respect to vehicles' desired speeds. However, the simulations can easily be expanded to also allow for heterogeneity in desired speeds.

We first compare the impact of the CF model on capturing vehicle behavior and the corresponding void creation (total void size created within platoon as a multiple of  $h_0$ ) and throughput reduction; see Fig 5-4. This was done in order to highlight how the results differ across the models. Newell's CF model results in the smallest total voids and CAB results in the largest, consistent with our expectation. The result suggests that Newell's CF model can greatly underestimate the amplification and propagation of disturbances. The AB model may also underestimate the impacts of a disturbance due to negligence of the second order effect (i.e.,  $\Delta \eta$  is positively correlated with  $\Delta v$  in the leader). It appears that the CAB model captures the different void creation effects more completely. The second order effect can be significant, evidenced by the sizable throughput reductions attributed to this effect.

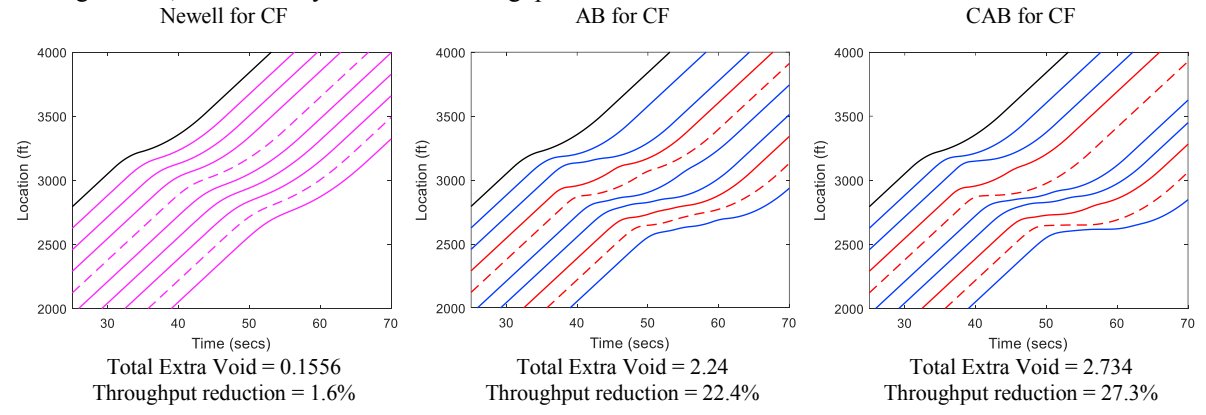


Fig 5-4: Generated platoon trajectories and total void created (as a multiple of  $h_0$ ) using Newell's simplified CF, AB Model, and CAB Model respectively. The colors represent the vehicle type / CF property (blue for convex pattern CAVs, red for concave RVs, and magenta for Newell). Heterogeneity in acceleration rates are depicted through solid lines for vehicles with high and dotted for vehicles with low desired acceleration.

In the third experiment, we further check if a dynamic acceleration, characterized by a dynamic acceleration model - a linear decay model (where desired acceleration rate linearly decreases with speed), has an impact on the void creation. For the same setup as in Fig 5-4, simulation was repeated two different acceleration models: (1) dynamic acceleration where  $a(v) = a_{max}(1 - 0.8(v/u))$  based on the TWOPAS model in (Allen et al., 2000) with slight modification, and (2) constant acceleration rate  $a(v) = a_{desired}$ , where  $a_{max}$  represents the maximal acceleration available for vehicle, and  $a_{desired}$  is an average desired acceleration rate. A factor 0.8 was introduced in the dynamic model so that vehicles can accelerate to u in finite time. We used a ratio of  $a_{desired} = a_{max}/1.5$  in the simulation<sup>†</sup>. Note that the acceleration model will have impacts in two aspects: (i) the initial void creation induced by the LC vehicle and (ii) void creation in the subsequent followers. For (i), the difference of void size between the two acceleration models depends on the inserting speed  $v_0$ . Specifically, if  $v_0$  is large (small), the dynamic model will create a larger (smaller) void. This is intuitive: consider a case that  $v_0 = 0.95u$ , the dynamic model will result in very small acceleration rates for  $v_0$  and higher speed, which will result in a large void. By contrast, if  $v_0 = 0.1u$ , dynamic model will result in much larger acceleration rates for most of the speed values when the vehicle increases from  $v_0$  to u. For (ii), the resulting void creation and throughput reduction are presented in Table 5-2. One can see that the dynamic acceleration model results in larger voids in both the AB and CAB models. On the other hand, the creation of additional voids is slightly reduced with Newell's model. However, the difference is very small and is more attributed to the randomness in generated acceleration rates and simulation error associated with discretization than the difference in how acceleration is modeled. Specifically, in the Newell setup, the void creation is strictly attributed to acceleration heterogeneity with the void being created only in front of the first slower accelerating vehicle in the platoon. The void therefore introduced due to the relative difference in acceleration rates between the vehicles. In the case of constant acceleration model, this difference is the entirety of the difference between their maximal acceleration rates. In the case of dynamic acceleration model, however, the absolute difference in average acceleration is less pronounced because each vehicle starts at speed greater than zero and hence  $a < a_{max}$ . Thus, it is possible that

<sup>&</sup>lt;sup>†</sup> Note: if  $a_{desired}$  uses the average acceleration across the time when a vehicle accelerates from 0 to u,  $a_{desired} = a_{max}/2$ . However, here we use  $a_{max}/1.5$  out of the consideration that vehicles will drive at moderate speed or higher for most time.

randomness in generated accelerations can overshadow the effect of difference in average acceleration. Nevertheless, we caution that the impacts of dynamic acceleration rate are complex as the acceleration can compound other parameters (e.g.  $v_0$ , reaction patterns, and level of acceleration heterogeneity across vehicles) and require further research.

Table 5-2: Total void created, and corresponding throughput reduction comparing the influence of acceleration model used, not including any voids created in front of the lead vehicle (such as voids created directly in front of LC vehicle).

	Newell	AB	CAB
Constant Accel	0.1556 (1.6%)	2.24 (22.4%)	2.734 (27.3%)
Dynamic Accel (Linear Decay)	0.1042 (1.0%)	2.5644 (25.6%)	3.2733 (32.7%)

It is important to note that in the results above, the quantitative values are sensitive to the choice of models (e.g., CF, acceleration models) and parameters used in the modeling. In our investigation, the seed values used for parameters related to the acceleration ranges and the CF behavior were purposely chosen to represent extreme (but still within realistic) ranges to highlight contrast, and thus might not represent common behavior observed in the field. A practitioner intending to use the model would be expected to carefully calibrate each parameter based on the field observations corresponding to the site of interest.

#### 6 Conclusions and discussions

This paper investigated the impacts of heterogeneity in driving behaviors under mixed traffic conditions, manifested in acceleration and CF behaviors, on traffic dynamics and throughput. The effects of each behavior were investigated analytically to unveil the impact mechanisms and then integrated to analyze the combined effects through simulations. Specifically, heterogeneity in the acceleration behavior involved differences in (preferred or maximum allowable) acceleration rate and desired speed among vehicles. We found that a smaller acceleration rate or desired speed imposes a constraint on traffic performance: (i) the first constraining vehicle, along the disturbance propagation path, with a smaller acceleration rate amplifies the disturbance and creates an additional void (if the LC vehicle has a larger acceleration); (ii) the additional void persists downstream if the vehicle has a smaller desired speed; otherwise gets shifted to the next constraining vehicle with smaller desired speed; and (iii) the magnitude of these effects depends on the LC vehicle's acceleration behavior. Moreover, through analytical formulation and numerical simulation, it was shown that mixed platoons resulted in larger voids than homogeneous platoons.

This paper also sheds light on heterogeneity in CF behavior, which manifests itself in the reaction pattern and sensitivity to a traffic disturbance. The former distinguishes between drivers that become aggressive and those that become timid as they navigate through a disturbance, while the latter introduces an additional dimension on a driver's reaction sensitivity to speed perturbance in its leader. The existing AB and CAB models for RVs were extended to capture the overall evolutionary pattern of CAV's response to a disturbance. With that, the behaviors of both RVs and CAVs can be represented by the unified frameworks (AB or/and CAB models). Typical reaction patterns were studied analytically to reveal insight on the mechanisms of void creations when the heterogeneity in CF behavior compounded heterogeneity in acceleration behavior. Specifically, it was shown that (1) finite acceleration, even though homogenous among vehicles, can contribute to void creation when it compounded certain reaction patterns in the deceleration process of CF; (2) heterogeneous accelerations resulted in larger total voids (compared to vehicles with homogeneous acceleration); and when heterogeneous CF and acceleration behaviors interact, they could compound the effects on void creation and result in larger voids. Finally, simulations that incorporated more detailed and realistic CF and acceleration behaviors (including different reaction patterns, correlation between  $\Delta \eta$  and  $\Delta v$ , and dynamic acceleration) were conducted to investigate the compounding effects on void creation and thus throughput reduction. The simulation results confirmed findings from the analytical investigation. Also, it was found that CAB model captures the different void creation effects more completely while Newell's CF model can significantly underestimate the void creation.

Note that this study aimed to provide physical insights into the impact mechanisms of heterogeneous vehicles on mixed traffic performance. As such, rather than tracking fine details of traffic dynamics, we made several simplifications and assumptions and limited the scope. Therefore, some limitations are notable and merit further research. For example, this study was concerned with the evolution of the void and disturbance created by a single LC vehicle and did not investigate interactions among multiple disturbances. The interaction is very complex even for homogenous vehicles (e.g., Chen and Ahn, 2018; Leclercq et al., 2011; Leclercq et al., 2016) and merits a more

systematic study in the future. Also, our simulations on the compounding effects only examined a limited number of scenarios. A more comprehensive analysis is needed to include more influential factors, such as (mainline and LC) flow, platoon size, and distribution of inter-platoon (or more generally inter-vehicle) gaps. In addition, more research is needed to examine the heterogeneity of CAV behavior in a more comprehensive manner considering different types of CAV control methods. Another issue is the acceleration models used. Limited by the scope of this paper, we only investigated a simple linear decay model, but the results suggest that the impacts of acceleration (i.e., dynamic vs. constant) were complex as acceleration can compound other parameters (e.g.  $v_0$ , reaction patterns, and level of acceleration heterogeneity across vehicles). Therefore, further research is needed to have a comprehensive investigation. The unifying frameworks provided in this paper can be used for this purpose. Furthermore, vehicle heterogeneity also affects disturbance propagations and results in changes in traffic properties (such as distribution of platoon size and composition), which is under investigation. An interesting application of the insights from this study would be to use the knowledge in developing vehicle control strategies (e.g., CAV longitudinal control) to improve traffic stability and efficiency. The basic analytical framework and the mechanisms learned from this study can serve as an important foundation for such endeavor. Finally, it is important to note that while the framework is presented with a focus on modeling mixed RV-CAV traffic, the framework can be generalized and used to study other forms of mixed traffic such as a mix of passenger cars and heavy vehicles as well.

## Acknowledgements

This research was sponsored by the United States National Science Foundation through CMMI Award 1536599.

#### References

- Aghabayk, K., Sarvi, M. and Young, W., 2015. A state-of-the-art review of car-following models with particular considerations of heavy vehicles. *Transport reviews*, 35(1), pp.82-105.
- Ahn, S. and Cassidy, M.J., 2007. Freeway traffic oscillations and vehicle lane-change maneuvers. In Transportation and Traffic Theory 2007. Papers Selected for Presentation at ISTTT17 Engineering and Physical Sciences Research Council (Great Britain) Rees Jeffreys Road Fund Transport Research Foundation TMS Consultancy Ove Arup and Partners, Hong Kong Transportation Planning (International) PTV AG.
- Allen, R.W., Harwood, D., Chrstos, J.P., Glauz, W.D., 2000. The Capability and Enhancement of VDANL and TWOPAS for Analyzing Vehicle Performance on Upgrades and Downgrades Within IHSDM. FHWA Publication No. 00-078.
- Bando, M., Hasebe, K., Nakanishi, K. and Nakayama, A., 1998. Analysis of optimal velocity model with explicit delay. *Physical Review E*, 58(5), p.5429.
- Bando, M., Hasebe, K., Nakayama, A., Shibata, A. and Sugiyama, Y., 1995. Dynamical model of traffic congestion and numerical simulation. *Physical review E*, 51(2), p.1035.
- Brackstone, M. and McDonald, M., 1999. Car-following: a historical review. Transportation Research Part F: Traffic Psychology and Behaviour, 2(4), pp.181-196.
- Chen, D. and Ahn, S., 2018. Capacity-drop at extended bottlenecks: Merge, diverge, and weave. Transportation Research Part B: Methodological, 108, pp.1-20.
- Chen, D., Ahn, S., Laval, J. and Zheng, Z., 2014. On the periodicity of traffic oscillations and capacity drop: the role of driver characteristics. Transportation research part B: methodological, 59, pp.117-136.
- Chen, D., Laval, J., Ahn, S. and Zheng, Z., 2012b. Microscopic traffic hysteresis in traffic oscillations: A behavioral perspective. *Transportation Research Part B: Methodological*, 46(10), pp.1440-1453.
- Chen, D., Laval, J., Zheng, Z. and Ahn, S., 2012a. A behavioral car-following model that captures traffic oscillations. Transportation research part B: methodological, 46(6), pp.744-761.
- Gao, W. and Jiang, Z.P., 2017. Nonlinear and adaptive suboptimal control of connected vehicles: A global adaptive dynamic programming approach. Journal of Intelligent & Robotic Systems, 85(2-4), pp.597-611.
- Gao, W., Jiang, Z.P. and Ozbay, K., 2017. Data-driven adaptive optimal control of connected vehicles. IEEE Transactions on Intelligent Transportation Systems, 18(5), pp.1122-1133.
- Gazis, D.C., Herman, R. and Rothery, R.W., 1961. Nonlinear follow-the-leader models of traffic flow. Operations research, 9(4), pp.545-567.
- Gipps, P.G., 1981. A behavioural car-following model for computer simulation. *Transportation Research Part B: Methodological*, 15(2), pp.105-111.
- Gong, S., Shen, J. and Du, L., 2016. Constrained optimization and distributed computation based car following control of a connected and autonomous vehicle platoon. Transportation Research Part B: Methodological, 94. pp.314-334.
- Hongfei, J., Zhicai, J. and Anning, N., 2003, October. Develop a car-following model using data collected by" five-wheel system". In Intelligent Transportation Systems, 2003. Proceedings. 2003 IEEE (Vol. 1, pp. 346-351). IEEE.
- Kesting, A., Treiber, M. and Helbing, D., 2010. Enhanced intelligent driver model to access the impact of driving strategies on traffic capacity. *Philosophical Transactions of the Royal Society of London A: Mathematical, Physical and Engineering Sciences*, 368(1928), pp.4585-4605.
- Kikuchi, S. and Chakroborty, P., 1992. Car-following model based on fuzzy inference system. Transportation Research Record, pp.82-82.
- Knoop, V., Hoogendoorn, S. and Adams, K., 2009. Capacity reductions at incidents sites on motorways. EJTIR, 4(9).

- Knoop, V., Hoogendoorn, S. and van Zuylen, H., 2008. Capacity reduction at incidents: empirical data collected from a helicopter. Transportation Research Record: Journal of the Transportation Research Board, (2071), pp.19-25.
- Kuderer, M., Gulati, S. and Burgard, W., 2015, May. Learning driving styles for autonomous vehicles from demonstration. In Robotics and Automation (ICRA), 2015 IEEE International Conference on (pp. 2641-2646).
- Laval, J.A. and Daganzo, C.F., 2006. Lane-changing in traffic streams. Transportation Research Part B: Methodological, 40(3), pp.251-264.
- Le Vine, S., Zolfaghari, A. and Polak, J., 2015. Autonomous cars: The tension between occupant experience and intersection capacity. *Transportation Research Part C: Emerging Technologies*, 52, pp.1-14.
- Leclercq, L., Knoop, V.L., Marczak, F. and Hoogendoorn, S.P., 2016. Capacity drops at merges: New analytical investigations. Transportation Research Part C: Emerging Technologies, 62, pp.171-181.
- Leclercq, L., Laval, J.A. and Chiabaut, N., 2011. Capacity drops at merges: An endogenous model. Transportation Research Part B: Methodological, 45(9), pp.1302-1313.
- Lee, H.D. and Sul, S.K., 1998. Fuzzy-logic-based torque control strategy for parallel-type hybrid electric vehicle. IEEE Transactions on Industrial Electronics, 45(4), pp.625-632.
- Lefèvre, S., Carvalho, A. and Borrelli, F., 2016. A learning-based framework for velocity control in autonomous driving. IEEE Transactions on Automation Science and Engineering, 13(1), pp.32-42.
- Ma, J., Li, X., Zhou, F., Hu, J. and Park, B.B., 2017. Parsimonious shooting heuristic for trajectory design of connected automated traffic part II: computational issues and optimization. Transportation Research Part B: Methodological, 95, pp.421-441.
- Mauch, M. and J. Cassidy, M., 2002, June. Freeway traffic oscillations: observations and predictions. In Transportation and Traffic Theory in the 21st Century: Proceedings of the 15th International Symposium on Transportation and Traffic Theory, Adelaide, Australia, 16-18 July 2002 (pp. 652-673). Emerald Group Publishing Limited.
- McDonald, M., Wu, J. and Brackstone, M., 1997, November. Development of a fuzzy logic based microscopic motorway simulation model. In Intelligent Transportation System, 1997. ITSC'97., IEEE Conference on (pp. 82-87). IEEE.
- Michaels, R.M., 1963. Perceptual factors in car-following. Proc. of 2nd ISTTF (London), pp.44-59.
- Morbidi, F. and Mariottini, G.L., 2013. Active target tracking and cooperative localization for teams of aerial vehicles. *IEEE transactions on control systems technology*, 21(5), pp.1694-1707.
- Naus, G.J., Vugts, R.P., Ploeg, J., van de Molengraft, M.J. and Steinbuch, M., 2010. String-stable CACC design and experimental validation: A frequency-domain approach. *IEEE Transactions on vehicular technology*, 59(9), pp.4268-4279.
- Newell, G.F., 1961. Nonlinear effects in the dynamics of car following. Operations research, 9(2), pp.209-229.
- Newell, G.F., 2002. A simplified car-following theory: a lower order model. *Transportation Research Part B: Methodological*, 36(3), pp.195-205. Öncü, S., Ploeg, J., Van de Wouw, N. and Nijmeijer, H., 2014. Cooperative adaptive cruise control: Network-aware analysis of string stability. *IEEE Transactions on Intelligent Transportation Systems*, 15(4), pp.1527-1537.
- Panwai, S. and Dia, H., 2007. Neural agent car-following models. IEEE Transactions on Intelligent Transportation Systems, 8(1), pp.60-70.
- Pipes, L.A., 1953. An operational analysis of traffic dynamics. Journal of applied physics, 24(3), pp.274-281.
- Pipes, L.A., 1966. Car following models and the fundamental diagram of road traffic. Transportation Research/UK/.
- Saad, F., Espie, S., Djemame, N., Schnetzler, B. and Bourlier, F., 1994. Microscopic traffic simulation and driver behavior modelling: The ARCHISIM Project. Road Safety in Europe and Strategic Highway Research Program (SHRP), Lille, France.
- Srivastava, A., Ahn, S., and Chen, D., 2019. CAV control to mitigate stop and go oscillations in mixed traffic with chained asymmetric driver behavior. *Working Paper*.
- Swaroop, D. and Hedrick, J.K., 1996. String stability of interconnected systems. IEEE transactions on automatic control, 41(3), pp.349-357.
- Swaroop, D.V.A.H.G., Hedrick, J.K., Chien, C.C. and Ioannou, P., 1994. A comparision of spacing and headway control laws for automatically controlled vehicles 1. *Vehicle System Dynamics*, 23(1), pp.597-625.
- Talebpour, A., Mahmassani, H. and Hamdar, S., 2011. Multiregime sequential risk-taking model of car-following behavior: specification, calibration, and sensitivity analysis. *Transportation Research Record: Journal of the Transportation Research Board*, (2260), pp.60-66.
- Wang, M., Daamen, W., Hoogendoorn, S.P. and van Arem, B., 2014. Rolling horizon control framework for driver assistance systems. Part I: Mathematical formulation and non-cooperative systems. Transportation research part C: emerging technologies, 40, pp.271-289.
- Wang, M., Daamen, W., Hoogendoorn, S.P. and van Arem, B., 2014. Rolling horizon control framework for driver assistance systems. Part II: Cooperative sensing and cooperative control. Transportation research part C: emerging technologies, 40, pp.290-311.
- Wiedemann, R., 1974. Simulation des Strassenverkehrsflusses. Technical report, Institut für Verkehrswesen, Universität Karlsruhe, Karlsruhe, Germany, In German.
- Zheng, Z., Ahn, S., Chen, D. and Laval, J., 2013. The effects of lane-changing on the immediate follower: Anticipation, relaxation, and change in driver characteristics. Transportation research part C: emerging technologies, 26, pp.367-379.
- Zhou, F., Li, X. and Ma, J., 2017. Parsimonious shooting heuristic for trajectory design of connected automated traffic part I: theoretical analysis with generalized time geography. Transportation Research Part B: Methodological, 95, pp.394-420.
- Zhou, M., Qu, X. and Li, X., 2017. A recurrent neural network based microscopic car following model to predict traffic oscillation. Transportation research part C: emerging technologies, 84, pp.245-264.
- Zhou, Y., Ahn, S., Chitturi, M. and Noyce, D.A., 2017. Rolling horizon stochastic optimal control strategy for ACC and CACC under uncertainty. *Transportation Research Part C: Emerging Technologies*, 83, pp.61-76.